

# Urban Area Unmanned Aerial Systems Sensor Capabilities for Ensuring Ground Hazards Safety

Xavier Bouyssounouse  
NASA Ames Research Center  
Moffett Field, CA  
xavier.bouyssounouse@nasa.gov

Corey Ippolito  
NASA Ames Research Center  
Moffett Field, CA  
corey.a.ippolito@nasa.gov

**Abstract**—Unmanned aerial systems (UASs) in urban areas can pose significant safety risks to dynamic ground objects (DGOs) such as people, pets, and bikes; especially for off-nominal emergency traverses and landings. This paper will examine a framework for evaluating the UAS safety benefits which can be achieved by classifying DGO hazards, modeling their behavior, and assigning collision costs. DGOs are assumed to be any ground objects which are either moving or capable of moving. Safety benefits will be assessed by analyzing metrics computed from UAS and DGO trajectories which take into account intent and uncertainties. This paper will establish the theoretical relationships mapping these trajectories and DGO classifications to safety levels. Sensor capabilities will be mapped to DGO trajectory uncertainties, so that safety can be directly estimated from the sensor specifications for a given UAS trajectory.

## I. INTRODUCTION

The overarching goal of this paper is to develop a framework for mapping Unmanned Aerial Vehicle (UAS) sensor and vision processing capabilities to Dynamic Ground Obstacle (DGO) safety. DGOs are assumed to be any ground objects which are either moving or capable of moving, and UAS are assumed to be CAT1 recreational, commercial, or emergency service aerial vehicles. Safety is maintained by ensuring the expected risk to all possible hazards stays below a maximum threshold.

$$\sum_i r_i < \delta \quad (1)$$

This equation is slightly misleading as written, because it does not explicitly show the correlation between potential incidents. For example, if there are two DGOs in the path of the UAS, and the UAS collides with the first DGO, then there is no longer a risk of collision with the second DGO unless it happens to be in close proximity to the first DGO. We will re-examine this equation later in this study after the discussion on likelihood probabilities.

Hazards are only considered if they can cause harm to people or property, while harm to the UAS itself is generally not considered in this study. The expected risk to the general public caused by hazard  $i$  can be computed by multiplying the consequence cost with the likelihood of that hazard occurring.

$$r_i = c_i \cdot l_i \quad (2)$$

Likelihoods and consequences will each be considered in depth in the following sections, and mathematical definitions

will be formulated so that they can be combined into an overall safety measure. Methods for minimizing the likelihoods and consequences will be discussed, and equations will be derived to establish the relationships between sensor specifications and safety. The effects of uncertainty in the trajectories and probabilities of the sensed DGO belonging to various classes will also be considered in this example. A methodology for analyzing the validity of the risk calculations will also be discussed.

## II. PREVIOUS WORK

The FAA Extension, Safety, and Security Act of 2016 [10] called for the Federal Aviation Administration (FAA) to “study the potential use of probabilistic assessments of risks by the Administration to streamline the integration of unmanned aircraft systems into the national airspace system.” Risk reduction models for addressing the FAA safety requirements include [1] and [6], and a comprehensive review of the state-of-the-art in UAS ground risk modeling has been analyzed in [11]. These risk models consider  $5 \times 5$  risk matrices such as [4] developed by the NASA Goddard Flight Center. However, these models do not drill down to the specific UAS sensor capability requirements, nor do they directly consider the DGO trajectories and uncertainties. Our paper complements these studies by showing how safety can be quantitatively measured given a specified UAS trajectory and a specified arrangement of DGOs. In order to form a mathematically analyzable model, we consider continuous likelihood and consequence values instead of the risk matrix referenced described above. For simplicity, we will only consider consequences of property damage and human harm, and risk will be assumed to be a simple product of likelihood and consequence.

## III. CONSEQUENCES

In the previous section we defined risk as the product of likelihood and consequence. Thus, it follows that risk can be reduced by either reducing the likelihood or reducing the consequence. In this section we will examine methods for reducing the consequences, and in the following section we will examine methods for reducing the likelihoods.

The consequence  $C_i$  associated with a hazard  $i$  can be estimated from insurance payouts, which are in turn based on the probabilities of causing serious injury or death. [9]

estimates these probabilities for human risk from a falling UAS based on kinetic energy at impact. These results can be readily generalized to include any UAS and DGO collision, provided the UAS weight and speed differential with the DGO can be estimated. Note that the safety consequence of crashing a UAS into the ground where no DGOs are present may indeed be essentially zero. However, as we will discuss further in the next section, the likelihood that there are no DGOs is never zero since no sensor is 100% reliable. Thus there will always be a predicted safety risk associated with any UAS crash.

We can examine how consequences can be reduced to ensure safety by considering a few examples. A DGO hazard involving a collision with a human can be described at varying levels of specificity, as illustrated in the notional example in figure 1. The high level hazard description shown in blue

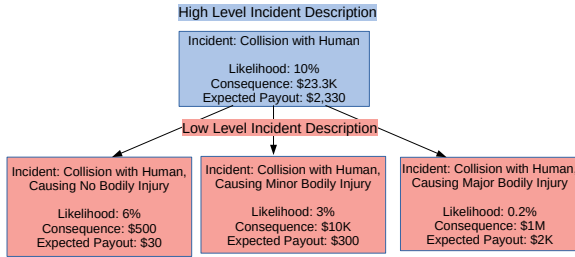


Fig. 1. Notional example showing high and low levels of hazard specificity.

can be broken down into three lower ones as shown in red, without affecting the total expected payout. If we examine the high level hazard description: “Collision with a human”, then clearly the consequence can be decreased if the UAS can be slowed down. However, if we look at the low level hazard description “Collision with a human causing major bodily injury”, then we can only change the likelihood (also by slowing down), but we cannot change the consequence. In general, it is clear that any hazard can be broken down into sub-hazard until the lowest level sub-hazard consequence cannot be changed. Therefore, we can state that the consequences  $C_i$  can never be decreased directly, and we must decrease the likelihoods in order to improve safety.

In summary, we have seen that the consequences are fixed costs when written at a sufficiently low level, and it is thus the likelihoods which must be lowered in order to improve safety. These fixed costs can be difficult to estimate (what is the cost of a human life?), however, studying insurance company incidence payouts and the methodologies they use to derive these payouts can help with the formulation of UAS and DGO collision consequence cost estimates.

#### IV. LIKELIHOODS

Likelihoods can be defined for our purposes as the probability that a hazard will result in a safety incident. Consider an initial UAS state of  $S_{UAS}(0)$ , and a target trajectory  $S_{UAS}(t)$ , given by

$$S_{UAS}(t) \equiv \{\mathbf{x}(t), \dot{\mathbf{x}}(t), \mathbf{w}(t), \dot{\mathbf{w}}(t)\}, \quad (3)$$

where

$$\mathbf{x}(t) \equiv \{x(t), y(t), z(t)\}^T, \quad (4)$$

is the position of the UAS and

$$\mathbf{w}(t) \equiv \{\alpha(t), \beta(t), \gamma(t)\}^T, \quad (5)$$

are the roll ( $\alpha$ ), pitch ( $\beta$ ), and yaw ( $\gamma$ ) of the UAS. A UAS will generally attempt to close the loop on its localization estimate to match a target trajectory  $S_{UAS}(t)$ . The UAS should be able to achieve position uncertainty similar to its localization uncertainty for low speed trajectories. However, these uncertainties will increase as the target UAS trajectories approach the aircraft performance model limits. Limitations in both UAS trajectory modeling and weather modeling will also increase the uncertainties. This is especially true for compromised UAS, since the performance models may be poorly understood. Compromised localization will make it harder to close the loop, also resulting in significantly increased uncertainties. Note that there is always a non-zero probability that a UAS will suddenly become compromised due to prop failure, sensor failure, etc. This is one of the main reasons why a UAS flying directly over DGOs is considered dangerous even though the planned trajectory does not bring the UAS anywhere near the DGOs. A realistic UAS trajectory estimator must thus also include these probabilities of failure along the routes. UAS Trajectory modeling is beyond the scope of this study, and we will assume that there exists a UAS trajectory modeler which can generate the possible trajectories with uncertainties, given an initial UAS aircraft state. Estimated UAS trajectories with uncertainties will be denoted by  $\hat{S}_{UAS}(t)$ , and estimated DGO trajectories can be similarly denoted by  $\hat{S}_{DGO}(t)$ .

Figure 2 shows notional UAS (red) and DGO (green) trajectories with  $1\sigma$  uncertainty errors. The specific shape of the DGO uncertainty will be described in detail later in this paper. We can write the position uncertainty of the UAS and

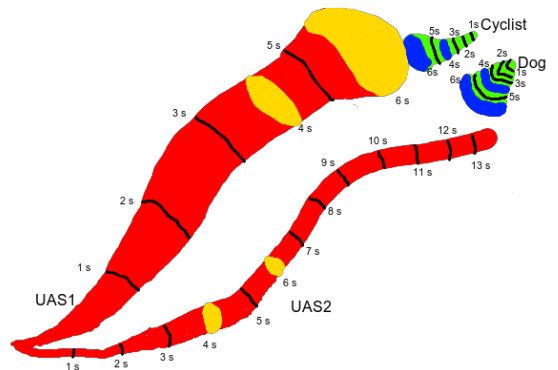


Fig. 2. Notional example showing predicted trajectories with  $1\sigma$  uncertainties. UAS trajectories are red, while DGO trajectories are green. Uncertainties at 4 and 6 second look-ahead are shown in yellow (UAS) and blue (DGO).

DGO at time  $t$  as three dimensional density function  $f_{UAS}(t, \vec{x})$  and  $f_{DGO}(t, \vec{x})$ , respectively. Note that the uncertainties and probability densities should be based on a local map, not on a global map, since the DGO predicted poses are based on

UAS sensor readings relative to the UAS. The term “local map” is used loosely here, as it might consist of a single reading from the mapping related sensors, or it could consist of multiple aligned readings to create a larger local map. These local maps might be registered against base maps to improve GPS localization, or perhaps these local maps are only used for local obstacle avoidance. For our analysis, we are primarily concerned with the DGO trajectories relative to the UAS.

Black lines are overlaid on the trajectories to show 1 second interval look-ahead times in figure 2. Note that UAS<sub>1</sub> has higher speeds than UAS<sub>2</sub>, and it is thus shown as having larger uncertainties since the implication is that it is flying closer to the edge of its modeled performance envelope. Note also that the cyclist is shown with a more predictable trajectory than the dog. We can calculate the likelihood of a collision between a UAS trajectory  $\hat{S}_{\text{UAS}}(t)$  and a DGO trajectory  $\hat{S}_{\text{DGO}}(t)$  by first considering the collision probability at a specific time. Consider the  $1\sigma$  uncertainties for the UAS (yellow) and DGO (blue) trajectories at 4 and 6 second look-ahead times in our notional example in figure 2. Note that the likelihood of collisions will be low at 4 seconds, however at 6 seconds the likelihood increases significantly for UAS<sub>1</sub> and the cyclist, with the  $1\sigma$  uncertainties butting up against each other.

The likelihood of a collision between a UAS trajectory and a DGO at a specific look-ahead time can be computed by point-wise multiplying the corresponding probability densities, and spatially integrating over the probability extent and over the geometric offsets where the UAS and DGO dimensions overlap. The geometric offset integration region can be understood by considering a fictitious example where the UAS and DGO each occupy single points in space. The trajectories between the UAS and DGO will then never actually overlap, and collisions will be impossible. However, as we consider real physical sizes it becomes clear that the actual size of the UAS and DGO must be considered in order to estimate the probabilities of collision.

A collision between a UAS and a DGO known to be of class  $i$  can be abbreviated as  $\text{UAS} \cap \text{DGO}_i$ . Thus the probability of this event occurring at time  $t$  can be written as

$$P_{\text{UAS} \cap \text{DGO}_i}(t) = \iint f_{\text{UAS}}(t, \vec{x} + \vec{r}) \cdot f_{\text{DGO}_i}(t, \vec{x}) d\vec{x} d\vec{r} \quad (6)$$

where  $f_{\text{UAS}}$  is the probability density of the UAS predicted trajectory,  $f_{\text{DGO}_i}$  is the probability density of the DGO predicted trajectory assuming it belongs to class  $i$ , and  $\vec{r}$  spans the geometric offsets as defined above.

A collision between a UAS and DGO where the DGO class is not known for certain can be abbreviated as  $\text{UAS} \cap \text{DGO}$ , and this probability can be calculated as:

$$P_{\text{UAS} \cap \text{DGO}}(t) = \sum_i [P_{i|\text{DGO}} \cdot P_{\text{UAS} \cap \text{DGO}_i}(t)] \quad (7)$$

where  $i$  iterates through all possible classes for the DGO,  $P_{i|\text{DGO}}$  is the probability that the observed DGO belongs to the class  $i$ . We can define  $t_C$  as the time of maximum probability of collision

$$t_C \equiv \underset{t}{\operatorname{argmax}} P_{\text{UAS} \cap \text{DGO}}(t) \quad (8)$$

Thus the probability of a collision with the DGO at any time along the UAS trajectory can be taken as the maximum probability of collision for any time:

$$P_{\text{UAS} \cap \text{DGO}} = P_{\text{UAS} \cap \text{DGO}}(t_C) \quad (9)$$

As mentioned briefly in the consequences section, there is always a non-zero probability that a collision with the ground will involve a DGO, since no sensor is 100% accurate in detecting all DGOs. We can thus include apriori density maps  $f_{\text{DGO}}$  in equation 6 for DGOs that might be present but have not necessarily been detected. These densities can either be non-spatially specific numbers based on expected densities of various DGO classes for the region, or the densities can be based on apriori maps, showing for example higher density of humans near bus stops and mall entrances, higher density of cattle in large fields, higher density of children near playgrounds, etc. [6] describes these scenarios in more detail. Note that these densities are based on a global map, not on the local maps used for the DGO densities. Thus, if a high resolution DGO population density map is required, then the UAS and DGO trajectories may need to be based off a global map by registering local maps against a base map. Including these densities in our risk calculations will result in a risk penalty even when no DGOs have been observed, which is what we want since we can never be 100% certain there are no DGOs.

So far we have considered the likelihood of a collision between a UAS and a single DGO. For multiple possible DGO collisions we must take into account the dependency between the collisions. For example, if a UAS collides with a DGO, then the probability of collision with future DGOs in its path is essentially zero, unless other UAS are nearby or if the UAS is not immediately grounded by the impact of the collision. We will make the simplifying assumption that any UAS crash grounds the UAS, making future crashes impossible. Thus, for multiple DGOs in the vicinity, the total probability of collision with any of the DGOs can be given by the sum of the disjoint probabilities:

$$\begin{aligned} & P(\text{UAS} \cap \text{Any DGO}) = \\ & P(\text{UAS} \cap \text{DGO}_1) + \sim P(\text{UAS} \cap \text{DGO}_1) \cdot P(\text{UAS} \cap \text{DGO}_2) + \dots \\ & = \sum_k \left[ P(\text{UAS} \cap \text{DGO}_k) \prod_{m=1}^{k-1} \sim P(\text{UAS} \cap \text{DGO}_m) \right] \quad (10) \end{aligned}$$

where the indexed DGOs in equation 10 refers to all the DGOs in the vicinity, with lower indices corresponding to DGOs earlier in the UAS path.

Note that the initial UAS trajectory point is very accurate since it is build from a local map. However, as look-ahead time increases, the performance modeling limitations increase the uncertainties, especially when flying near the performance model limits. Note also that even with perfect localization and sensors, there is still a chance of a sudden UAS failure which increases over time, thus the uncertainties will grow over time. The initial DGO uncertainty is due to the sensor limitations,

which will be analyzed later in this paper. However, as the look-ahead time increases, the DGO uncertainties are dominated by the DGO intent modeling limitations.

## V. RISK

Recall that the risk associated with a hazard is the product of the likelihood and the consequence, as given in equation 2. Consider again the consequence of a collision  $C_i$  between a UAS and DGO. These collision consequence costs will be greater at higher speed differentials, and can be worse if the UAS is spinning (say due to failed props). Thus the consequence between a UAS and a DGO can be written with explicit state dependencies as:

$$\text{Collision Consequence: } C(\text{DGO}_i, \hat{S}_{\text{UAS}}(t_C), \hat{S}_{\text{DGO}_i}(t_C))$$

where  $\text{DGO}_i$  represents a DGO of class  $i$ ,  $\hat{S}$  represents the UAS and DGO states defined in equation 3, and  $t_C$  is the collision time as defined in equation 8. We will abbreviate this collision consequence to  $C(i, t_C)$ . Thus, the risk associated with a single DGO collision can be written as

$$R(\text{UAS} \cap \text{DGO}) = \sum_i [P_{\text{UAS} \cap \text{DGO}_i}(t_C) \cdot C(i, t_C)] \quad (11)$$

and the risk associated with any DGO collision in the vicinity can be written as:

$$R(\text{UAS} \cap \text{Any DGO}) = \sum_k \left[ C_k \cdot P(\text{UAS} \cap \text{DGO}_k) \prod_{m=1}^{k-1} \sim P(\text{UAS} \cap \text{DGO}_m) \right] \quad (12)$$

where  $C(k, t_C)$  has been abbreviated to  $C_k$ .

Thus, the original risk equation given in equation 1 with collision dependencies can be written as:

$$R(\text{UAS} \cap \text{Any DGO}) < \delta, \quad (13)$$

We have thus shown how safety can be computed for a specific UAS trajectory and a set of DGOs with uncertainty values. A UAS with presumed trajectory estimators can then plan its path based on its own set of mission costs, so long as equation 13 can be satisfied. In the event that there are no possible trajectories whose risk remains below this threshold, then the UAS should be considered in safety violation, and should chose the trajectory which minimizes the risk.

## VI. DGO TRAJECTORY MODELING

The DGO trajectories will be modeled as dead reckoned trajectories with velocity uncertainties that depend on the detected object class probabilities. For example, a small child running would have relatively high velocity uncertainty, while an adult cyclist would have considerably less velocity uncertainty. Holonomic constraints which could affect along track and cross track uncertainties differently will not be considered. Complex DGO trajectory prediction based on planning and goal modeling such as [5] is beyond the scope of our study.

DGOs will generally have very little rotational velocities, so these will not be model-led. For simplicity, DGOs will assume to be restricted to flat motion along the ground. The DGO state trajectory can thus be simplified from equation 3 to

$$\mathbf{x}(t) \equiv [x(t) \ y(t) \ \dot{x}(t) \ \dot{y}(t)]^T \quad (14)$$

The dynamics can be modeled as a discrete linear dynamic system

$$\mathbf{x}_{k+1} = F\mathbf{x}_k + \xi, \quad (15)$$

with the initial state given as

$$\mathbf{x}_0 \equiv [x_0 \ y_0 \ z_0 \ \dot{x}_0 \ \dot{y}_0 \ \dot{z}_0]^T \quad (16)$$

and  $F$  is the state transition matrix given by

$$F = \begin{bmatrix} 1 & 0 & 0 & \Delta t & 0 & 0 \\ 0 & 1 & 0 & 0 & \Delta t & 0 \\ 0 & 0 & 1 & 0 & 0 & \Delta t \\ 0 & 0 & 0 & 1 & 0 & 0 \\ 0 & 0 & 0 & 0 & 1 & 0 \\ 0 & 0 & 0 & 0 & 0 & 1 \end{bmatrix} \quad (17)$$

with update period  $\Delta t$ , and  $\xi$  drawn from a normal distribution

$$\xi \sim \mathcal{N}(\mathbf{0}, Q) \quad (18)$$

with

$$Q = \begin{bmatrix} 0 & 0 & 0 & 0 & 0 \\ 0 & 0 & 0 & 0 & 0 \\ 0 & 0 & q & 0 & 0 \\ 0 & 0 & 0 & q & 0 \\ 0 & 0 & 0 & 0 & 0 \end{bmatrix} \quad (19)$$

The initial state  $\mathbf{x}_0$  will have uncertainties that depend on the UAS sensor capabilities, while the velocity uncertainty  $q$  will vary depending on the object class. Note that even a single DGO detected by the UAS will have to consider multiple possible trajectories, weighted by the classification confidences  $P_{i|\text{DGO}}$ , as shown in equation 7. Multiple detected DGOs will need to use equation 10.

## VII. ESTIMATING DGO TRAJECTORY UNCERTAINTY FROM SENSOR SPECIFICATIONS

The DGO position and speed relative to the UAS is assumed to be measured with stereo cameras on the UAS, and these measurements will have inherent uncertainty associated with the 3D reconstruction. Other sensors such as LIDAR and SONAR can be quite useful for measuring position and speed, depending on the size and payload capabilities of the UAS. However, for the scope of this study we will restrict our analysis to stereo cameras, and this work should be easily extendable to other sensors. In this section we will explore how these inherent stereo uncertainties map into trajectory uncertainties. It can be shown [8] and [2] that the stereo range error due to discretization of the image pixels is related to the pixel disparity error by:

$$\Delta z = \frac{-z^2 \Delta d}{bf + z \Delta d}, \quad (20)$$

where  $\Delta z$  is the range error,  $b$  is the camera baseline,  $f$  is the focal length, and  $\Delta d$  is the pixel disparity error.

The pixel disparity error probability distribution function depends on the physical properties of the sensor. For example, if we assume the camera sensor can capture light uniformly over the entire span of each pixel, then a uniformly distributed disparity error density function is reasonable for both the left and right cameras, as used in [8]. Other density function such as a triangular shaped curve have been explored by [2]. For this study, we will assume that the pixel disparity error is uniformly distributed over one pixel. The probability density functions for the left image pixel disparity error is given by:

$$f_{\Delta x_L}(\Delta x_L) = \begin{cases} 1/\delta, & \text{for } -\delta/2 \leq \Delta x_L \leq \delta/2 \\ 0, & \text{otherwise} \end{cases} \quad (21)$$

where  $\delta$  is the image pixel size. The probability density function for the right image pixel disparity error is similarly given by:

$$f_{\Delta x_R}(\Delta x_R) = \begin{cases} 1/\delta, & \text{for } -\delta/2 \leq \Delta x_R \leq \delta/2 \\ 0, & \text{otherwise} \end{cases} \quad (22)$$

Thus, since the disparity error  $\Delta d$  is the sum of the left and right disparity errors, we can calculate the probability density function for  $\Delta d$  as the convolution of the left and right probability density functions:

$$f_{\Delta D}(\Delta d) = f_{\Delta x_L}(\Delta x_L) * f_{\Delta x_R}(\Delta x_R), \quad (23)$$

which integrates to:

$$f_{\Delta D}(\Delta d) = \begin{cases} (\delta + \Delta d)/\delta^2, & \text{for } -\delta \leq \Delta d \leq 0 \\ (\delta - \Delta d)/\delta^2, & \text{for } 0 \leq \Delta d \leq \delta \\ 0, & \text{otherwise} \end{cases} \quad (24)$$

Clearly a larger disparity error will result in a larger range error estimate, and thus  $\Delta z$  is a monotonic function of  $z$ , so we can write

$$f_{\Delta Z}(\Delta z | z) = f_{\Delta D}(\Delta d) \left| \frac{\partial}{\partial \Delta z}(\Delta d) \right| \\ = \frac{bf}{(z + \Delta z)^2} \cdot \begin{cases} (\delta + \Delta d)/\delta^2 & \text{for } -\delta \leq \Delta d \leq 0 \\ (\delta - \Delta d)/\delta^2, & \text{for } 0 \leq \Delta d \leq \delta \\ 0, & \text{otherwise} \end{cases} \quad (25)$$

These equations map stereo camera focal length, pixel size, and baseline to the probability density functions of the DGO range errors for stereo cameras. The horizontal and vertical errors orthogonal to range have been shown by [3] to have minimal error contribution compared to range, and will thus be ignored in this paper. Thus, we can calculate the total DGO trajectory uncertainties by adding range errors to the DGO trajectories modeled in equation 14. Stereo camera resolution will affect the DGOs visible in the field of view, while frame rate will affect motion blur and maximum speeds.

Similar calculations can be performed for LIDAR. Flash LIDAR is particularly simple because the range errors are

constant up to the maximum range. Note that regardless of the sensor used, the DGO uncertainties due to intent will quickly grow over time, and will dominate all uncertainties except for very short look-ahead times.

## VIII. METRICS FOR EVALUATING RISK VALIDITY

Equation 12 demonstrates how risk can be calculated between a UAS trajectory and a set of DGO trajectories, given several simplifying assumptions. These assumptions include stereo cameras as the only sensor for range estimation and object recognition, and dead reckoned DGO velocity estimates that assume DGO intent is unaffected by nearby UASs. So far we have not addressed how to validate that the risk equations are relevant given these assumptions.

Recall that risk is the product of consequences and likelihoods. Validating that the consequences are correct is not straight forward. In some sense they are correct by definition. The insurance payouts can be used as a starting point to set the consequence costs, but it is ultimately up to the FAA regulators to decide the true consequence costs based on policy priorities. Thus, we will focus our risk validity to the likelihood calculations.

Perhaps the equations given in 12 are too simple to correctly capture the risk or perhaps they are overly complex given the uncertainty in the system, or more likely they are some combination of both.

The following are examples where the system could be overly complex for the risk calculations:

- Object class is not a good predictor of the dead reckon uncertainties.
- DGO intent is so unpredictable that motion estimation based on object class are unreliable.

The following are examples where a more complex system might better capture risk:

- DGO intent could consider short term variations in motion to better predict future motions.
- Tracking a DGO for a short term would also provide better robustness for object classification.
- DGO intent could include higher order terms beyond simple dead reckoning. For example, a person identified as digging a ditch.
- UAS failure modes may need to be improved to better capture risk.

The collision probability given in 10 can be converted to a binary classifier by considering that a collision is predicted so long as the probability is above a threshold. A low threshold will increase the probability of the correct detections while simultaneously increasing the probability of false positives, while a high threshold will lower both. This relationship between the true positive rate and the false positive rate can be traced in an ROC curve by varying the threshold. However, the true positives and false positives calculations require real data of actual UAS and DGO collisions, which can be difficult to obtain. Assuming we can obtain this data, then the quality of our classifier can be estimated by calculating the area

under the ROC curve. A value of 1.0 represents a perfect assignment of collision probabilities, 0.5 representing a pure random assignment of collision probabilities, 0.0 representing an inverted classifier with perfect incorrect classification. We can thus demonstrate the effects of changes to our probability equations from a variety of factors including the ones proposed in the itemized list at the beginning of this section. This method permits us to discard irrelevant elements collision probability while retaining and expanding those elements which can improve performance.

### IX. SUMMARY AND FUTURE WORK

This paper developed the risk models in equations 12 and 13 for ensuring safety to DGOs, and described how these risks models could be validated and improved given real-world data. The greatest source of uncertainty is intent of the dynamic ground objects, however it is difficult to collect real data of collisions or near misses because these occurrences are infrequent and can have privacy sensitivities. For our analysis we have assumed that the object intent is not affected by the UAS proximity. This simplifies the risk equations and permits real data to be collected in future studies, with the UAS and DGOs completely separated spatially and temporally. Equation 25 would then be used to scale the results as the UAS and DGOs are relocated to simulate near misses and collisions.

Our first order approximation where DGOs do not react to the UASs will not be valid under all scenarios. In many cases, collisions and near misses happen so quickly that the DGOs do not have time to react. This is especially true in busy urban areas where the UAS may not be heard coming. If the UAS is noticed, then adults are most likely going to try to avoid a collision. However, pets and children may be far less predictable, and may attempt to chase the UAS. These highly complex interactions are important to model because they can predict when our UAS and DGO interaction simplifying assumptions are valid. Studying these interactions can also help generate intent models that can be used to improve risk prediction. Statistics on these interactions can help identify when the predicted DGO motion is too unreliable and a simple worst case motion model must be used. Real-world data of collisions and near misses is difficult to obtain because they do not occur often and also because there may be privacy or other sensitivities associated with these occurrences. Future work could attempt to collect this hard to collect data of near misses and collisions.

The risk equations have assumed stereo cameras would be used for range estimation. This work can be readily augmented to cover a variety of other sensors such as LIDAR and SONAR, with only the range estimation noise models given in equation 25 requiring updating. Object tracking could significantly improve the classification of DGOs since some objects are not easily recognizable from certain views.

A simulation environment can be invaluable for testing out end-to-end workflow for the risk calculations, and isolating the effects of intent modeling assumptions, and sensor and algorithm selection. A simulation environment was readily setup

using the ROS Gazebo environment as shown in figure 3. This example simulate the third person view and telemetry from the stereo cameras and flight control system. For this example, a 3DR Robotics Iris UAS was simulated with a Pixhawk PX4 flight controller, noisy inertial navigation system, and random wind gusts. The simulation includes buildings, moving cars,



Fig. 3. ROS Gazebo Simulation Environment, combining the Gazebo vehicle and city simulation environment, and the Pixhawk PX4 Flight controller.

and several dynamic models of people walking, jogging, and talking with hand gestures. Sun, shadows, and clouds are also modeled. The simulated UAS is equipped with stereo cameras which are used to classify DGOs and estimate their position and velocity relative to the UAS. A GPU based real-time object classifier [7] is incorporated into this simulation, as shown in figure 4 to determine the DGO class based on training data

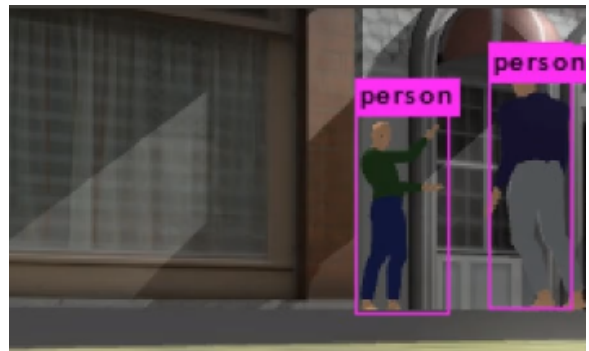


Fig. 4. Example of the “You Only Look Once” real-time object classifier running on our simulated UAS camera view.

of the expected classes for the UAS region. A real-time 3D optical flow object motion estimation algorithm such as [12] can also be incorporated into the simulation to estimate the velocity of DGO objects.

This paper is primarily targeted at class I UAVs, however these results are readily applicable to larger aircraft, since the main changes would be the trajectory modeler and the addition of more sophisticated sensors. It is hoped that this paper can provide a structured framework to build upon for evaluating the risks UAS pose to DGOs.

## REFERENCES

- [1] *Assessing the risks of integrating unmanned aircraft systems (UAS) into the National Airspace System*. The National Academies Press, Washington, DC, 2018.
- [2] R. Balasubramanian, S. Das, S. Udayabaskaran, and K. Swaminathan. Quantization error in stereo imaging systems. *International Journal of Computer Mathematics*, 79(6):671–691, 2002.
- [3] S. D. Blostein and T. S. Huang. Error analysis in stereo determination of 3-d point positions. *IEEE Transactions on Pattern Analysis and Machine Intelligence*, PAMI-9(6):752–765, Nov 1987.
- [4] G. S. F. Center. Goddard technical standard, risk management reporting, 2009.
- [5] K. Ehsani, H. Bagherinezhad, J. Redmon, R. Mottaghi, and A. Farhadi. Who let the dogs out? modeling dog behavior from visual data. *CoRR*, abs/1803.10827, 2018.
- [6] C. A. Ippolito. Dynamic ground risk mitigation for autonomous small uas in urban environments. *AIAA Scitech Forum*, 2019.
- [7] J. Redmon, S. K. Divvala, R. B. Girshick, and A. Farhadi. You only look once: Unified, real-time object detection. *CoRR*, abs/1506.02640, 2015.
- [8] J. J. Rodriguez and J. K. Aggarwal. Quantization error in stereo imaging. pages 153–158, June 1988.
- [9] A. Shelley. A model of human harm from a falling unmanned aircraft: Implications for uas regulation. *International Journal of Aviation, Aeronautics, and Aerospace*, 3, 01 2016.
- [10] R. P. J. Tiberi. H.r.636 - faa extension, safety, and security act of 2016, 2016.
- [11] A. Washington, R. Clothier, and J. Silva. A review of unmanned aircraft system ground risk models. *Progress in Aerospace Sciences*, 95, 11 2017.
- [12] A. Wedel and D. Cremers. *Stereoscopic Scene Flow for 3D Motion Analysis*. Springer, 2011.